Structural, electrical and optical studies on AgI–anatase composites

2003 J. Phys.: Condens. Matter 15 5057

(http://iopscience.iop.org/0953-8984/15/29/317)

INSTITUTE OF PHYSICS PUBLISHING JOURNAL OF PHYSICS: CONDENSED MATTER

J. Phys.: Condens. Matter **15** (2003) 5057–5072 PII: S0953-8984(03)60976-8

Structural, electrical and optical studies on AgI–anatase composites

Shosuke Mochizuki[1] **and Fumito Fujishiro**

Department of Physics, College of Humanities and Sciences, Nihon University, 3-25-40 Sakurajosui, Setagaya-ku, Tokyo 156-8550, Japan

E-mail: motizuki@physics.chs.nihon-u.ac.jp

Received 18 March 2003, in final form 3 June 2003
Published 11 July 2003
Online at stacks.iop.org/JPhysCM/15/5057

Abstract

AgI–anatase composites, (x)AgI–$(1-x)$anatase, were fabricated over a wide composition range of 0–100% AgI for the first time. The electrical conductivity at 300 K increases with increasing AgI content and reaches a maximum (about 3×10^{-2} S m^{-1}) at about 40% AgI. The conductivity is enhanced by about three orders of magnitude in comparison with that of pristine AgI. These composite specimens have been characterized by both scanning electron microscopy and x-ray diffractometry. The observations with a scanning electron microscope show that anatase fine particles are densely packed in an AgI particle of several micrometres in size and such composite particles are three-dimensionally connected to each other to form a composite specimen. The photoluminescence (PL), PL excitation and time-resolved PL spectra of these composites have also been measured at different temperatures between 8 and 278 K. The exciton spectra obtained related to the anatase particles and the AgI domains in anatase-packed AgI particles are discussed in the light of the morphological, structural and conductivity data.

1. Introduction

There has been considerable experimental research on ionic conduction in composite solid electrolytes consisting of ionic conductors and insulator fine particles (Liang 1973, West 1984, Shahi and Wagner 1981, Zhao *et al* 1983, Lee *et al* 2000a). The electrical and other properties of the composites can be easily controlled by varying the content of the ionic conductor component. Among various systems of composites, AgI-based composites have been extensively investigated by many workers, because they usually show high ionic conductivity ($\sigma \geqslant 10^{-2}$ S m^{-1}) and pristine AgI is well known as a good superionic conductor at temperatures higher than 420 K (Burley 1963). AgI has three phases designated as α, β and

[1] Author to whom any correspondence should be addressed.

γ at normal pressures in the order of decreasing temperature with the following properties. At the superionic transition temperature T_c (420 K), the superionic α phase transforms into the semiconductor β phase (wurtzite lattice). The α phase has a body-centred cubic arrangement of I^- ions with highly mobile Ag^+ ions randomly distributed through the equivalent interstices, which has been known as the averaged structure. At room temperature, the semiconductor γ phase (zincblende lattice) appears as a metastable state. It is said that the stability of the γ phase is affected by slight nonstoichiometries and other defects. To date, the conductivity of AgI-oxide fine particle composites has been reported in various composites: AgI–Al_2O_3, AgI–SiO_2, AgI–MgO, AgI–Fe_2O_3 (Shahi and Wagner 1981, Zhao *et al* 1983), AgI–ZrO_2, AgI–CeO_2, AgI–Sm_2O_3, AgI–MoO_3, AgI–WO_3 (Shastry and Rao 1992) and AgI–SnO_2 (Gupta *et al* 1996). In all these cases, their electrical conductivities were enhanced by two or three orders of magnitude higher than that of pristine AgI and a maximum conductivity occurred at proper AgI content. For example, the maximum occurs in (x)AgI–$(1-x)\gamma Al_2O_3$ composites with very fine alumina particles at $x = 0.5$–0.6, while composites with larger alumina particles showed the maximum at smaller AgI content. Such conductivity variation is initially explained by taking into account a space charge layer around a nucleophilic surface (Jow and Wagner 1979). However, several basic problems were raised about AgI-based composites. Why do oxides enhance the conductivity? How does AgI attach to oxide fine particles? What are the atomic and electronic structures of the AgI/insulator fine particle interface? In order to solve these problems, it is thought that optical study is effective. Constituent material AgI shows clear optical spectra due to excitons in the bulk (Mochizuki and Fujishiro 2002), films (Cardona 1963, Mochizuki and Ohta 2000) and microcrystals (Mochizuki and Umezawa 1997). Besides AgI, most oxides also show exciton spectra. The exciton behaviour is very sensitive to the environment in which excitons are moving, and therefore the optical spectra due to excitons may provide useful information about the AgI/oxide fine particle interface (Mochizuki and Fujishiro 2003). Very recently, we have fabricated AgI–anatase composites and observed considerable conductivity enhancement. Since AgI is very photosensitive and anatase (TiO_2) is known as a typical oxide photocatalyst for decomposing water and organic matter (Fujishima *et al* 2000), we can anticipate not only a new solid electrolyte nature but also a new photofunction for such an AgI–anatase fine particle composite.

In this paper, we report the morphological, structural, electrical and optical studies on AgI–anatase composites and we discuss the conductivity enhancement of the composites by comparing the scanning electron microscope images with the data obtained.

2. Experimental details

AgI–anatase composites, (x)AgI–$(1-x)$ anatase, were prepared by fully mixing AgI powder and amorphous titanium dioxide fine particles (with an average diameter of 50 nm) in air, heating the mixture in the lidded crucible at 673 K for 12 h in air and then annealing at 373 K for 12 h to remove the stress introduced at the phase transition point of AgI, 420 K. The composition range was from 0 to 100% AgI. At 300 K, the composites were characterized by x-ray diffraction (XRD) analysis with Cu Kα_1 radiation. The composite powder morphology was studied by a scanning electron microscope (SEM) and an optical microscope with a charge-coupled device camera system. Distribution maps of Ag, I, Ti and O atoms in the composites were obtained by using a SEM with an energy dispersive x-ray (EDX) fluorescence spectrophotometer (Shimadzu SSX-550).

Electrical conductivity measurements were performed in a helium gas stream using the impedance method. The applied signal frequency ranged from 42 Hz to 1 MHz. The composite powders were uniaxially compressed under 0.2 GPa for 30 min at room temperature to fabricate

pellets. It has been reported that the γAgI/βAgI ratio is strongly affected by compressing, grinding and the thermal history of specimens. Such an effect, a so-called memory effect, is erased by heat treatment above 445 K (Bloch and Möller 1931, Burley 1967). Therefore, the pellets were heat-treated at 453 K for 12 h in a lidded crucible and then annealled at 373 K for 12 h. Electrical contact with the pellets was obtained by evaporating silver onto both sides of the pellet.

The photoluminescence (PL) spectra were measured by an optical multichannel analyser consisting of a grating monochromator (focal length = 32 cm) and an intensified diode-array detector (gate time: $t_g \geqslant 5$ ns). A Nd^{3+}:YAG laser (wavelength $\lambda = 355$ nm, pulse width < 5 ns) and a monochromatic light source consisting of a 150 W xenon lamp and a grating monochromator (focal length = 20 cm) were used as the excitation source. The photoluminescence excitation (PLE) spectra were recorded by varying the excitation-light wavelength λ_{ex} with an apparatus consisting of the same monochromatic light source described above and detecting the emission light intensity at the desired wavelength as a function of λ_{ex} with a grating monochromator (focal length = 20 cm) and a synchronous light detection system. The time-resolved PL (TRPL) spectra were taken using the same optical multichannel analyser to which two delay pulse generators were attached. The delay time t_d and gate time were set with these delay pulse generators which were controlled by a personal computer. A closed-cycle He refrigerator equipped with a temperature controller was used to change the specimen temperature between 8 and 278 K.

3. Results and discussion

3.1. Characterization of AgI–anatase composite specimens

The apparent density of the (x)AgI–$(1 - x)$anatase composites at about 300 K is plotted, together with the theoretical density, as a function of AgI content x in figure 1. The full line and full circles represent the theoretical and experimental (observed) densities, respectively. Theoretical densities were calculated by using the reported densities of pristine AgI (5960 kg m^{-3}) and pristine anatase (3880 kg m^{-3}). The porosity variation with x is shown in the inset. A remarkable difference between the theoretical and experimental density is observed in the smaller x region. Such a result is known behaviour for the compaction of mixtures of particles with extremely different hardnesses. The porosity variation with x may affect the apparent conductivity of the composites.

We studied the surface morphology of (x)AgI–$(1 - x)$anatase specimens by SEM observations both on the raw surfaces and the fractured ones. Figures 2(a) and (b) show, respectively, the low- and high-magnification SEM images for the surface of the (0.4)AgI–(0.6)anatase composite. The EDX fluorescence measurements indicate that large particles and small particles are AgI and anatase, respectively. As seen in these figures, anatase fine particles are densely packed in AgI particles of several micrometres in size. Henceforth, we call this particle the 'anatase-packed AgI particle'. As shown in these figures, small anatase particles are not so different in size from the initial average particle size of 50 nm, while other anatase particles coagulate to form irregularly shaped particles of several hundred nanometres in size. The EDX fluorescence measurements indicate that iodine-rich parts tend to appear inside pore walls and that the surroundings of anatase particles are silver-rich. The latter suggests that Ag^+ ions are adsorbed onto the anatase particle surfaces.

Figure 3 shows the XRD patterns of (x)AgI–$(1 - x)$anatase composites at 300 K. All XRD patterns in this figure are normalized at the peak intensity. Amorphous titanium dioxide powder, as one of the starting materials, was fully transformed into crystalline anatase by

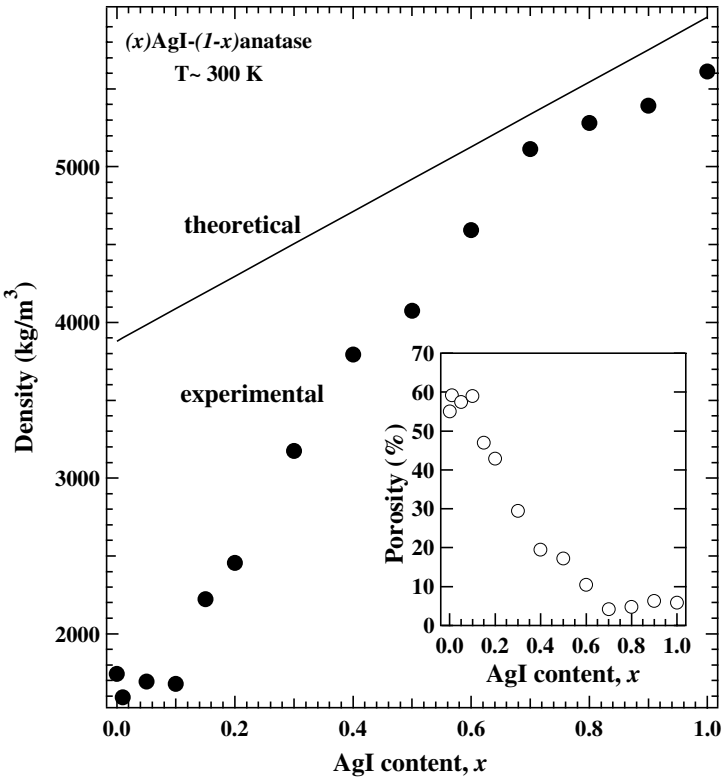

Figure 1. Density of different (x)AgI–$(1-x)$anatase composites at about 300 K. Porosity variation with x is shown in the inset.

heating at 673 K in air for 12 h. With increasing x, some diffraction lines related to AgI become pronounced. All diffraction lines can be almost assigned to γAgI, βAgI and anatase. It seems to be a mere mixture of AgI and anatase. This is very different from that observed in AgI–γAl_2O_3 composites (Lee *et al* 2000a, Mochizuki and Fujishiro 2003). In the AgI–γAl_2O_3 composites, some broadening of the peaks and weakening of the (h0l) and (100) peaks of βAgI become pronounced with increasing x, and some new diffraction lines appear. The new lines can be explained by taking account of the seven-hexagonal-layer polytype AgI (7H-AgI) with the stacking sequence ABCBCAC (Lee *et al* 2000a, 2000b). In the present AgI–anatase composites, however, such polytype-structure lines as observed in AgI–γAl_2O_3 composites never appear, as shown in the inset. In the inset, the full curve represents the XRD pattern of the (0.7)AgI–(0.3)anatase composite, while the broken curve represents that of the (0.73)AgI–(0.27) γAl_2O_3 composite which displays clear (1010) and (1011) lines of the polytype structure. Some broadening is also observed on the βAgI (100) and (002) lines for the small x region. Such line broadening becomes diminished with increasing x. The broadening may arise mainly from reduced crystallite size. The intensity ratio of the βAgI (002) line, which coincides with the γ (111) peak to the βAgI (100) line, increases from 1.919 to 3.384 with increasing x from 0.2 to 0.8. Such an increase may be explained by either a preferred orientation of βAgI crystallites or an increased γAgI component in the anatase-packed AgI particles, accompanied by stacking disorder in hexagonal βAgI. However, it is noted that the βAgI (101), βAgI (102) and βAgI (103) lines almost disappear, while the γAgI (331) line becomes sharpened with

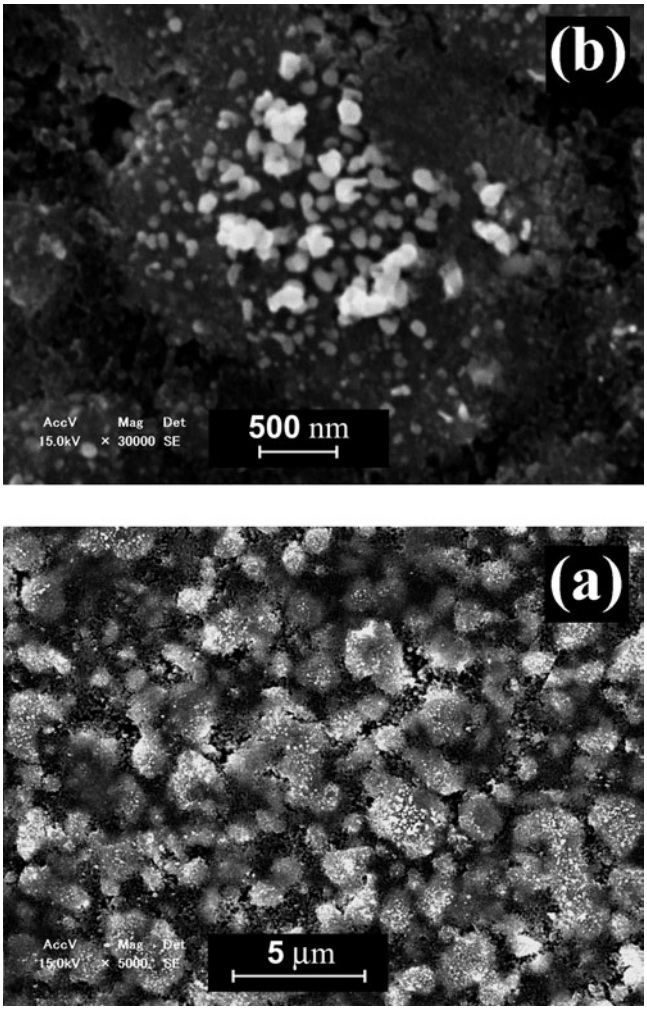

Figure 2. SEM image of the (0.4)AgI–(0.6)anatase: (a) at low magnification (×5000), (b) at high magnification (×30 000).

increasing x, as shown in figure 3. Therefore, to explain the XRD patterns obtained, the contribution from the increased γAgI component should be more taken into account than the preferred orientation. In other words, the AgI domain in the anatase-packed AgI particles consists of many γAgI crystallites and a small number of βAgI crystallites. Referring to the known result that a silver-deficient AgI solution crystallizes in the β phase and silver-rich AgI solutions do so in the γ phase, this is interpreted as follows. Preferential Ag^+ ion adsorption on anatase surfaces, as shown in the SEM and EDX fluorescence data, induces some concentration gradient of Ag^+ ions in the AgI domain. The gradient produces then γAgI crystallites and βAgI ones in the AgI domain. The degree of the gradient is dependent on the anatase content and, therefore, the diffraction intensity ratio of the γAgI line and the βAgI line varies with x, as shown in figure 3. On the other hand, the linewidth of the broad anatase (101) line is found to be almost independent of x. It may indicate that the average size of the anatase particle is not considerably changed by heating. This is consistent with the SEM observation shown in figures 2(a) and (b).

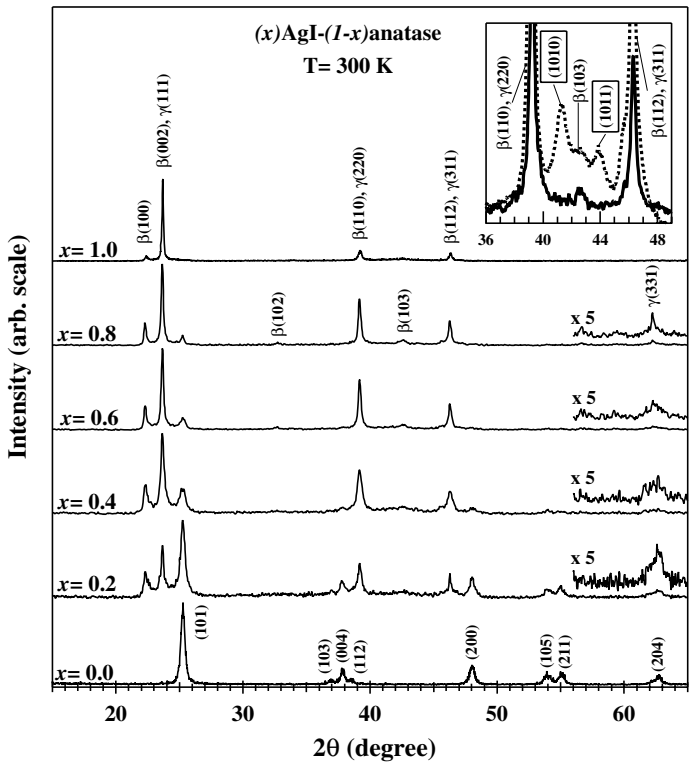

Figure 3. XRD patterns for different (x)AgI–$(1-x)$anatase composites at 300 K. The XRD pattern for (0.7)AgI–(0.3)anatase (full curve) is compared with that for (0.73)AgI–(0.27)γAl_2O_3 (broken curve) in the inset.

3.2. Electrical conductivity

The conductivity σ of (x)AgI–$(1-x)$anatase composites at 300 K is plotted against x in figure 4. The applied frequency was 1 kHz. No frequency dependence of σ was observed between 42 Hz and 100 kHz. Because of experimental difficulties, the transference numbers for ionic and electronic charge carriers have not been directly determined. However, tentative measurements on the transient current of the asymmetric cell of type $(Ag/(x)AgI–(1-x)anatase/Au)$ show a small steady-state current. Therefore, we cannot perfectly exclude the contribution from electronic conduction from the present discussion. As seen in this figure, σ increases abruptly with increasing x. On further increasing x, σ reaches a maximum (about 3×10^{-2} S m^{-1}) at $x = 0.4$. Since the σ for a pristine AgI specimen prepared in the same way is 1.7×10^{-5} S m^{-1}, the conductivity is enhanced by about three orders of magnitude. In the x region larger than 0.4, σ falls gradually toward 1.7×10^{-5} S m^{-1} for pristine AgI. The maximum σ is close to that observed in the AgI–γAl_2O_3 composite (Uvarov *et al* 2000). Through the present measurements of σ at different temperatures, the following are also found about (x)AgI–$(1-x)$anatase composites:

(1) The σ varies exponentially with temperature below 373 K, while the activation energy for the pristine AgI specimen rises continuously from 0.35 to 0.99 eV with increasing temperature from 300 to 400 K. The activation energy E_σ below 400 K is plotted against x in the inset. The broken curve is the least-squares fit for the plotted E_σ.

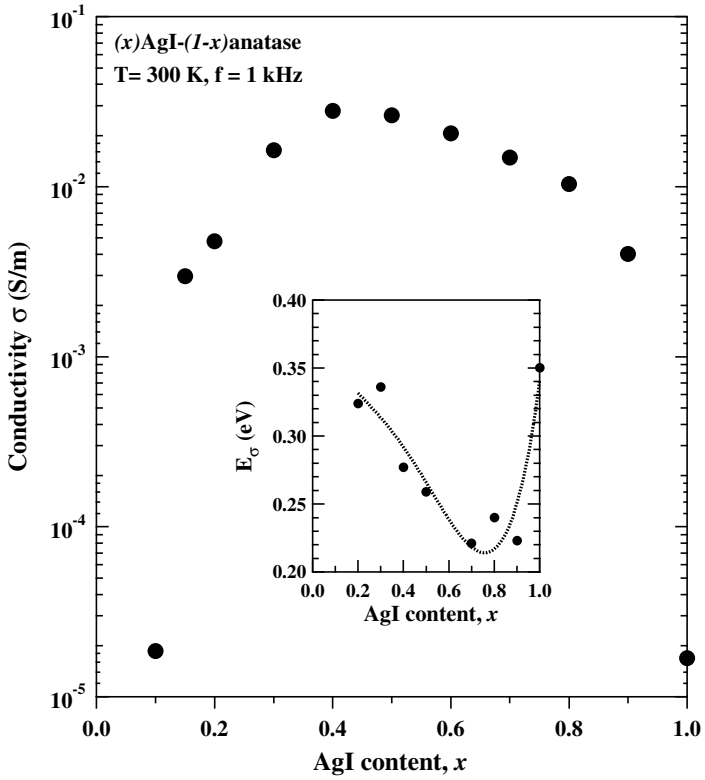

Figure 4. Conductivity of different (x)AgI–$(1-x)$anatase composites at 300 K. The applied frequency was 1 kHz. The activation energy E_σ below 400 K is plotted against x in the inset. The broken curve is the least-squares fit for the plotted E_σ.

(2) The σ at room temperature is not considerably changed for a heating–cooling cycle below T_c.
(3) The composite with larger x ($\geqslant$0.4) exhibits more clearly an abrupt σ change near the T_c (420 K) of pristine AgI with some accompanying transition hysteresis, as observed in the AgI–γ Al_2O_3 composite (Lee *et al* 2000a).

In the light of the porosity data shown in figure 1, the σ variation in the small x region ($x \ll 0.4$) may be mainly caused by the insulating pore effect. On the other hand, the conductivity enhancement observed in the large x region ($\geqslant$0.4) may arise from some composite effects, since the starting materials, pristine AgI and anatase, have low conductivities. The composite effects arise from highly ionic-conductive regions at the AgI/anatase interfaces and γAgI/βAgI interfaces in anatase-packed AgI particles. It is known that the adsorption of Ag^+ ions at insulating oxide surfaces leads to the formation of vacancies on Ag^+ sites and the space charge layer. As referred to already in section 3.1, it is also known that a silver-rich AgI solution crystallizes in the γ phase, while a silver-deficient solution crystallizes in the β phase. The γAgI and βAgI crystallites may act as Ag^+ ion donor and acceptor, respectively. Thus, we can anticipate high Ag^+ ion conductivity at the γAgI/βAgI interfaces in anatase-packed AgI particles. With decreasing x from 1 to 0.4, dispersed anatase particles approach each other and then the space charge effect spreads over the AgI domain to display a maximum in the σ–x curve. The activation energy E_σ for σ shows a complicated x

dependence, as shown in the inset of figure 4. The least-squares fitting curve (broken curve) for E_σ exhibits a minimum near $x = 0.7$. It is noted that the porosity variation with x exhibits also a minimum near the same x, as shown in the inset of figure 1. The E_σ of 0.35 eV for the present pristine AgI is smaller than 0.38 eV for an ordered βAgI crystal. This may be explained by the extensive disorder of Ag^+ ions in the stacking faulted structure and such a disordered arrangement of Ag^+ ions may provide a higher energy state than in the ordered βAgI structure with a decrease of E_σ (Lee *et al* 2000b). By adding anatase particles to the pristine AgI, the E_σ decreases. This indicates a generation of new ionic transport pathways. This is due to Ag^+ ion adsorption onto anatase fine particles. On further adding anatase, E_σ becomes affected by both the electronic conduction in anatase particles and the existence of insulating pores. Following more detailed discussion, the transference numbers for ionic and electronic charge carriers should be determined.

The effects of crystalline defects introduced by some strain coming from stress with different thermal expansion coefficients between AgI and anatase should also be taken into consideration (Jow and Wagner 1979).

3.3. Optical spectra

Before describing the results of optical measurements on (x)AgI–$(1-x)$anatase composites, we point out general photoinduced properties obtained for AgI-based glasses (AgI–$AgPO_3$ glasses, AgI–Ag_2MO_4 and AgI–Ag_2WO_4) and AgI-based composites (AgI–γAl_2O_3 and AgI–ZnO (Fujishiro and Mochizuki 2003)). These AgI-based ionic conductors are easily blackened with intense ultraviolet laser light. Such blackening becomes prominent with increasing temperature and increasing AgI content. The blackening is due to precipitation of silver clusters or silver fine particles, which is an irreversible reaction. The blackening gives rise to PL intensity reductions, which is the so-called photodarkening. Therefore, we checked the blackening by examining the reproducibility of measured PL spectra at different laser fluences and then we found a suitable excitation light intensity for the PL measurement for each specimen.

In figure 5, the PL spectra obtained for (x)AgI–$(1-x)$anatase composites with different compositions at 8 K are compared. The PL was excited by the 355 nm laser line of the Nd^{3+}:YAG laser. All spectra in this figure are normalized at the peak intensity. Pristine anatase shows a broad PL band centred at about 536 nm (2.31 eV) with a large Stokes shift of 0.89 eV. The present PLE spectrum measurement of this broad PL band at 8 K shows a sharp PLE edge, corresponding to the optical absorption edge, at about 3.2 eV which is close to the bandgap energy of pristine anatase. This PL band has been tentatively assigned to the radiative recombination of self-trapped excitons in pristine anatase by many authors (Tang *et al* 1994, Hosaka *et al* 1997, Suisalu *et al* 1998). The addition of a small amount of AgI, $x = 0.2$, leads to a considerable decrease of this anatase PL and gives a sharp PL band at 428 nm with accompanying shoulders at about 423 nm and about 438 nm. The spectrum is affected by noise at wavelengths shorter than 415 nm. The decreased PL intensity of the 536 nm band is due to the absorption of excitation laser light by the AgI domain in an anatase-packed AgI particle. In pristine AgI, the bands at about 424 nm and about 429 nm are assigned to the radiative recombination of $Z_{1,2}$ excitons and shallowly trapped $Z_{1,2}$ ones, respectively (Mochizuki and Fujishiro 2002, Cardona 1963, Mochizuki and Ohta 2000, Mochizuki 2001, Mochizuki and Umezawa 1997). No measurable spectral change with x is observed in the 536 nm band. Further addition of AgI, $x = 0.4$, increases the longer wavelength sideband to generate a broad band centred at 442 nm and reduces the 536 nm band, with an accompanying slight bandwidth narrowing at the longer wavelength side ($\lambda > 536$ nm). On further increasing x

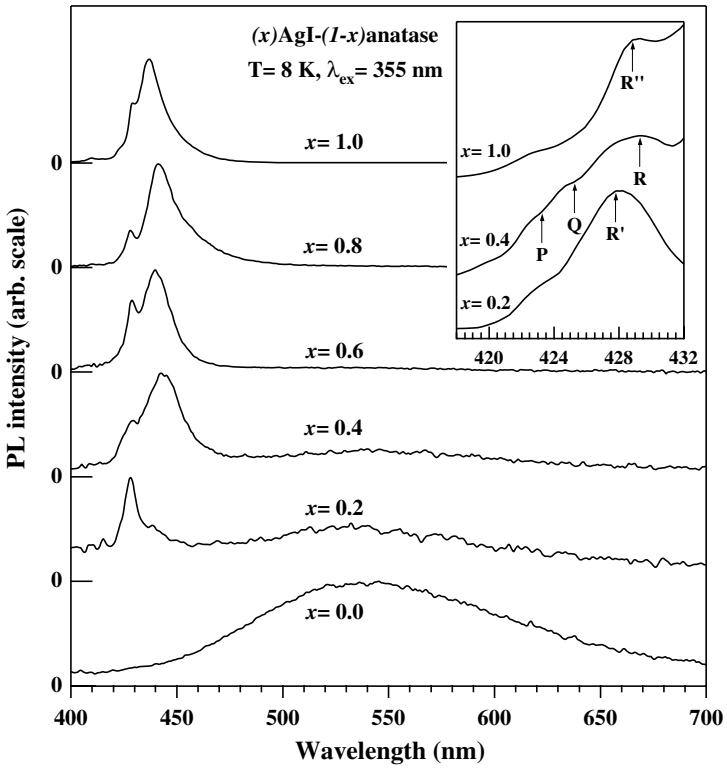

Figure 5. PL spectra of different (x)AgI–$(1-x)$anatase composites at 8 K. Free exciton PL bands for (0.2)AgI–(0.8)anatase, (0.4)AgI–(0.6)anatase and pristine AgI are shown in the inset. The PL bands labelled R, R′ and R″ are due to radiative decays of shallowly trapped excitons.

from 0.4 to 0.8, this broad band becomes narrowed and blue-shifted to 441 nm, which is close to the intensity maximum (437 nm) of pristine AgI. Therefore, it should be interpreted that the broad band consists of the 438 and 442 nm bands. We interpret the observed spectral variation with x, as follows. In the specimens with smaller x, since free excitons are confined in smaller AgI domains, excitons reach AgI domain surfaces and AgI/anatase interfaces and then decay radiatively. Since the energy bandgap (about 3.1 eV) of AgI is close to that (3.2 eV) of anatase, the potential for trapping free AgI excitons is thought to be shallow. In such a case, unlike the AgI–γ Al_2O_3 composite (Mochizuki and Fujishiro 2003), any PL band due to radiative decay of excitons deeply trapped at the AgI/anatase interfaces may not be apparently observed, as shown in figure 5. However, as described below, a small number of excitons deeply trapped at the AgI/anatase interfaces are found through measurements of the excitation-light intensity dependence of the PL spectrum. It should also be pointed out that the fine structure at the higher energy side of the 429 nm band becomes prominent at $x = 0.4$. In the inset, the higher energy side spectral structure for the (0.2)AgI–(0.8)anatase and (0.4)AgI–(0.6)anatase composites is compared with that for the pristine AgI specimen which was prepared in the same way. The shoulders at about 423 nm and about 425 nm, which are respectively labelled P and Q, are seen for the (0.4)AgI–(0.6)anatase composite. As shown in the inset of figure 6, both the P and Q shoulders remain clearly even at 129 K (=11.1 meV) in spite of the small energy separation (13.8 meV) between P and Q. With increasing x, the P and Q shoulders tend to move toward about 424 nm. The $Z_{1,2}$ exciton originates from the doubly degenerate valence band

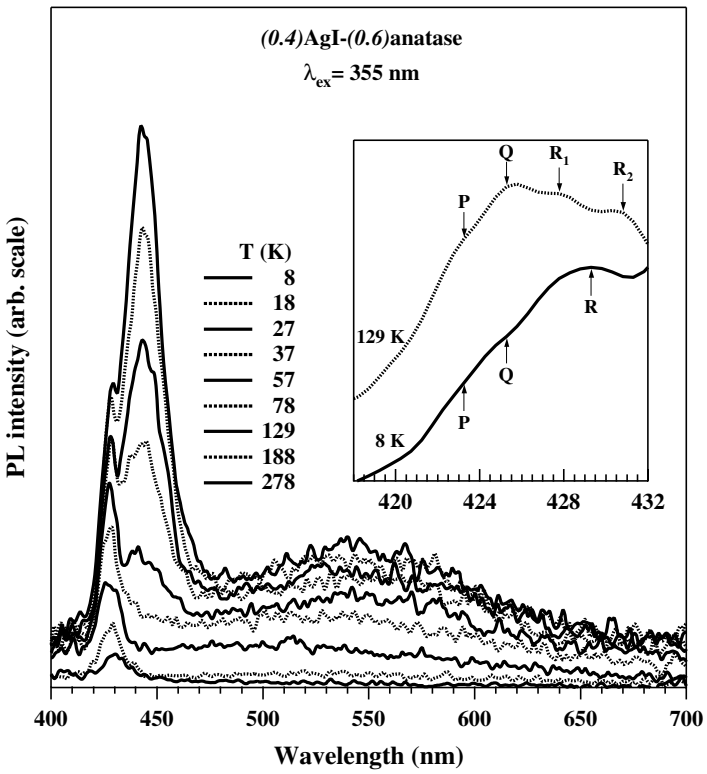

Figure 6. Temperature dependence of the PL spectrum of the (0.4)AgI–(0.6)anatase composite. The temperature increases in the curves from top to bottom. The PL spectra at 8 and 129 K are compared in the inset by rescaling their intensities.

Γ_8 with light and heavy hole masses. The Γ_8 band tends to split by some crystal-field change caused by mixing with the wurtzite structure or some internal stress caused by different thermal expansion coefficients between the AgI and anatase. Therefore, such Γ_8 splitting should be taken into account for rigorous assignment of the 423 and 425 nm shoulder bands. Such an exciton spectrum is similar to that of the microcrystal specimen (Mochizuki and Umezawa 1997). The spectral structure of the 429 nm peak (labelled R) assigned to shallowly trapped $Z_{1,2}$ excitons changes with x as shown in the inset. The changed bands are labelled R′ and R″. This indicates that there are several shallowly trapped exciton states. In such cases, the lower energy trapped excitons tend to populate higher energy trapped exciton states with increasing temperature.

The PL spectra of AgI–anatase composites were studied at different temperatures between 8 and 278 K. The result obtained for the (0.4)AgI–(0.6)anatase composite with maximum σ is shown in figure 6 as a typical example. In comparison with the emission intensities of the P-, Q- and R-emission shoulders, the emission of the 442 nm band decreases prominently with increasing temperature. The intensity peak at about 442 nm was assigned above to radiative decay of excitons trapped by lattice defects and impurities in the AgI domain. On further increasing temperature above 78 K, the 442 nm band almost disappears and absolutely disappears at 278 K. Above 188 K, the intrinsic and extrinsic exciton bands are slightly red-shifted, which is ascribed to the decrease of the bandgap energy of AgI with increasing temperature. Such a redshift was also observed at pristine AgI (Mochizuki and Ohta 2000).

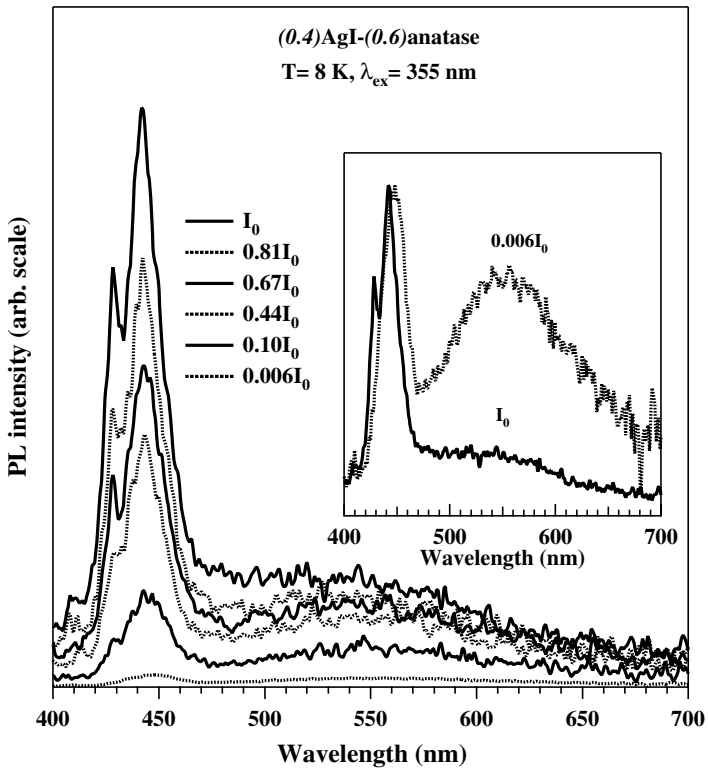

Figure 7. Excitation-light intensity dependence of the (0.4)AgI–(0.6)anatase composite at 8 K. The laser fluence increases in the curves from top to bottom. The PL spectra for the weakest and most intense excitations are compared by rescaling their intensities in the inset.

The disappearance of the 442 nm band may be due to a thermally activated reverse process from trapped states to free exciton ones. The 536 nm band becomes weaker and shifted to shorter wavelength with increasing temperature. Such a blueshift was also observed in the pristine anatase specimen. This indicates the decreased exciton-lattice relaxation energy. As described later, the broad 536 nm band consists of two bands. If these bands have different temperature dependences, such a blueshift of the 536 nm band is possible. The PL intensity decrease of the 536 nm band with increasing temperature from 8 to 98 K is about two times larger than that observed in pristine anatase. This may be attributed to the exciton trapping and nonradiative exciton decay at the AgI/anatase interface.

The excitation-light intensity I_{ex} dependence of the PL spectrum is also studied at 8 K on different (x)AgI–$(1-x)$anatase composites. The result obtained for the (0.4)AgI–(0.6)anatase composite with maximum σ is shown in figure 7 as a typical example. With decreasing laser fluence, the free exciton P- and Q- shoulder emissions and the shallowly trapped exciton R emission decrease linearly with I_{ex}. On the other hand, the 442 and 536 nm emissions decease nonlinearly with decreasing I_{ex}, but their decreases are smaller than those of the P, Q and R emissions. Upon further decreasing I_{ex}, the 536 nm emission intensity becomes comparable to that of the 442 nm emission with accompanying intensity peak wavelength shift from 536 to 552 nm. This indicates that the 442 and 536 nm emissions have higher yields than the free exciton emissions and the shallowly trapped exciton emission. But the 442 and 536 nm emissions become saturated under intense excitation. These saturations arise from a finite

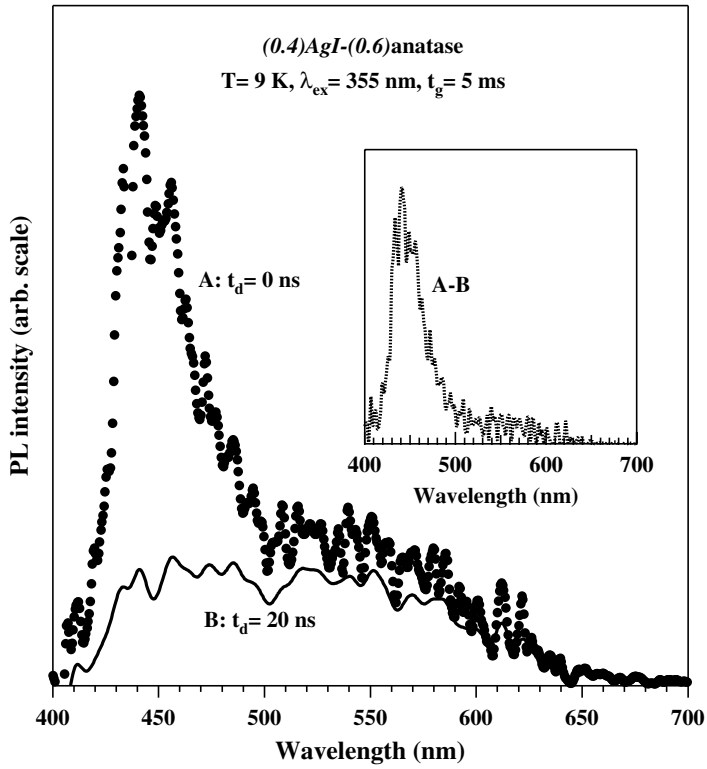

Figure 8. TRPL spectrum of the (0.4)AgI–(0.6)anatase composite at 9 K. Curves A and B correspond to the time-resolved spectra integrated from 0 ns to 5000 μs and integrated from 20 ns to 5000.02 μs after incidence of the laser pulse, respectively. The PL component (curve A − curve B) for short delay time is shown in the inset.

number of shallow- and deep-level PL centres. In the inset, the PL spectra observed under intense ($I_0 = 33$ mJ cm^{-2}) and weak ($0.006I_0$) excitations at 8 K are compared. We have assigned tentatively the 536 nm band to radiative decay of self-trapped excitons in pristine anatase on the basis of both the present PLE spectrum edge (about 3.2 eV) and the assignment made previously in several papers (Tang *et al* 1994, Hosaka *et al* 1997). However, the PL intensity of the composite saturates at a laser fluence larger than 33 mJ cm^{-2}, while we cannot detect any saturation in pristine anatase particles. Therefore, the results may indicate that the excitons in anatase are affected by adding AgI. Deeply trapped excitons in anatase may be formed by exciton–phonon interactions or by interactions between free electrons and trapped holes by defects at the AgI/anatase interfaces or both. Since the number of defects is limited, the emission from such deeply trapped excitons at the interfaces becomes saturated under intense excitation. The observed redshift from 536 to 552 nm with decreasing I_{ex} may indicate that anatase-related emission consists of at least two emission bands, labelled as X and Y bands.

The TRPL spectra of AgI–anatase composites were measured at 9 K. Since the TRPL measurements need longer data-acquisition times and the composites easily became blackened by excitation laser light during the measurements, as stated above, we considerably reduced the laser fluence. As a result, the spectra are considerably affected by noise. In figure 8, the TRPL spectra at 9 K shown for the (0.4)AgI–(0.6)anatase composite with maximum σ are typical

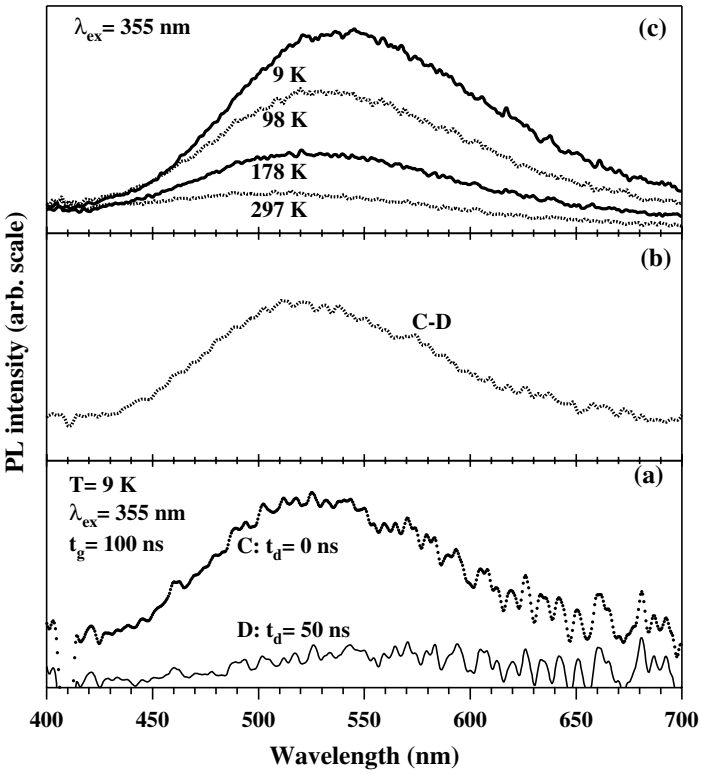

Figure 9. PL spectra of pristine anatase fine particles at 9 K: (a) TRPL spectra, (b) short-delay-time emission, (c) temperature dependence of the PL spectrum.

examples. Curves A and B correspond to the time-resolved spectra integrated from 0 ns to 5000 μs and integrated from 20 ns to 5000.02 μs after incidence of a laser pulse, respectively. At a first glance, the PL spectrum consists of a broad band due to anatase shown as the bottom curve and another broad band due to AgI. In order to extract the short-delay component, we have calculated the difference spectrum (curve A − curve B). The result (curve A–B) is shown in the inset. The difference spectrum gives an image of the 'pure' short-time emission spectrum. Comparing this difference spectrum with those of pristine AgI and pristine anatase shown in figure 5, one can identify the short-time emission spectrum made up essentially of several kinds of AgI-related emission (400 nm $< \lambda <$ 500 nm) and weak anatase-related emission (500 nm $< \lambda <$ 700 nm). On the other hand, the long-time emission spectrum (full curve) may be anatase-related emission, which consists of two components centred at about 465 nm and about 536 nm.

The TRPL spectra of pristine anatase particles are also measured at 9 K. The results are given in figure 9(a). Curves C and D correspond to the time-resolved spectra integrated from 0 to 100 ns and integrated from 50 to 150 ns after incidence of the laser pulse, respectively. In order to extract the short-delay component, we have calculated the difference spectrum (curve C − curve D). The result is shown in figure 9(b). The short time emission (curve C–D) is blue-shifted in comparison with the long-time emission (curve D). The blue-shifted emission indicates that the broad band emission of pristine anatase particles consists of different radiative decays of self-trapped excitons. The PL spectrum of the same pristine anatase specimen was also

measured at different temperatures between 9 and 297 K. The results are shown in figure 9(c). As seen in this figure, the broad PL band is blue-shifted with increasing temperature. This may be related to the above-mentioned multicomponent of the PL band. We should note the spectral structure difference between curve B in figure 8 and curve D in figure 9(a). We compared the PL and TRPL spectra of (0.4)AgI–(0.6)anatase with those of pristine anatase particles and single crystals (Tang *et al* 1994, Watanabe *et al* 2000). In the result, we have reached a view that anatase-related excitons are partially trapped at the AgI/anatase interface. Since an exciton trap is closely related to a defect, the view may yield a conclusion that there are defects at the AgI/anatase interfaces. Assuming that the effect is explained as a space charge effect, the probable reason is the adsorption of Ag^+ ions at the thereby positively charged oxide surfaces and the creation of numerous vacancies at the AgI/anatase interfaces. When the interface has a comparatively large defect density, the interface region may have high ionic conductivity. The detailed report on the PL and TRPL studies on various pristine anatase specimens will be presented in a separate paper (Mochizuki *et al* 2003).

We have already discussed the space charge effects at the AgI/anatase interfaces on ionic conduction. We need to discuss such space charge effects on excitons. The space charges generate a potential gradient, namely an electric field, which drives the self-trapped exciton formation, exciton trapping and exciton dissociation.

4. Conclusion and remarks

The results obtained for (x)AgI–$(1-x)$anatase composites are briefly summarized as follows.

(1) Conductivity enhancement higher than three orders of magnitude is observed.
(2) The SEM and EDX fluorescence measurements indicate that anatase fine particles are packed in large AgI particles of several micrometres in size and such anatase-packed AgI particles are three dimensionally connected to form a composite specimen. We named these composites particles anatase-packed AgI particles. Silver-rich parts appear around anatase particles. This indicates Ag^+ ion adsorption on the surfaces of the anatase particles. The measurements indicate also that some of the anatase particles are nearly isolated and others aggregate with each other to form larger particles.
(3) The XRD pattern of AgI domains in anatase-packed AgI particles is similar to that of type II AgI crystals (Lee *et al* 2000b) and the (311) line of γAgI is observed. The AgI domain in the anatase-packed AgI particles consists of γAgI and βAgI crystallites.
(4) The splitting of the $Z_{1,2}$ exciton spectra of AgI is observed as two shoulder PL bands. These may arise from some crystal-field change caused by the mixing with the wurtzite structure or some internal stress caused by different thermal expansion coefficients between the AgI and anatase.
(5) The anatase-related exciton spectra in the anatase-packed AgI particles are considerably affected in comparison with pristine anatase. Excitons in anatase fine particles are partially trapped at the AgI/anatase interfaces which may contain numerous crystalline defects.

Results (2) and (3) explain well the observed conductivity data for (x)AgI–$(1-x)$anatase composites. It may be concluded that adding anatase fine particles to AgI produces vacancies on Ag^+ ion sites, a space charge layer and a heterostructure for γAgI and βAgI crystallites. In such anatase-packed AgI particles, both the AgI/anatase interface regions of neighbouring anatase particles and the γAgI/βAgI crystallite interfaces would provide pathways for high conductivity.

The main limitation of our technique is that there are no direct mesoscopically space-resolved electrical and optical measurements on the composite specimens. Bearing this

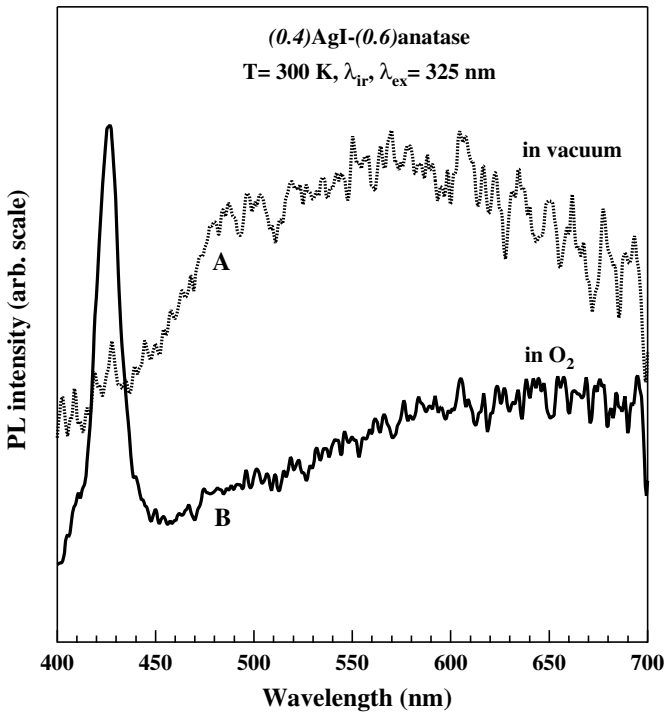

Figure 10. Reversible photoinduced spectral change in (0.4)AgI–(0.6)anatase composites at 300 K. Both the irradiation laser light wavelength λ_{ir} and the PLE laser light wavelength λ_{ex} are the same: 325 nm.

limitation in mind, we have presented some reasonable connections between the measured data and composite effects in the AgI–anatase system. With a near-field optical microscope measurement system and a SEM, the space-resolved optical and structural measurements on different AgI–oxide systems are now in progress in our laboratory.

Very recently, we have measured the Raman scattering spectra of (x)AgI–$(1-x)$ anatase composites at room temperature. The present pristine AgI shows a broad band centred at 88 cm^{-1}. This band is assigned to extra modes coming from defects. When x is decreased to less than 0.2, the band shifts to 78 cm^{-1} and becomes resolved into three bands centred at about 68, 78 and 94 cm^{-1}. Such a spectral change may give more directly information about the defect structure at AgI/anatase interfaces (Mochizuki *et al* 2003).

Finally, we have very recently found a reversible photoinduced spectral change in the present (x)AgI–$(1-x)$anatase composite specimens at room temperature. The spectral change obtained for (0.4)AgI–(0.6)anatase is shown in figure 10 as a typical result. After fully irradiating at 300 K with 325 nm laser light in a vacuum specimen chamber, the specimen shows a broad PL spectrum (curve A) due to trapped excitons in anatase. Oxygen gas is then introduced into the chamber. With increasing irradiation time, the broad PL band becomes weak, while a sharp PL band due to the excitons in AgI grows at 426 nm and the broad PL band prevails, as indicated by curve B. The chamber is again evacuated. The broad PL spectrum reappears. It is found through many successive experiments that the spectral changes appear repeatedly. The enhancement of the broad PL is related to photogenerated oxygen vacancies and is observed for many oxides, for example Eu_2O_3, Sm_2O_3 (Mochizuki *et al* 2001a, 2001b) and SiO_2 (Mochizuki and Araki 2003). The observed spectral changes

may originate from the photoinduced dissociative adsorption and photoinduced associative detachment of O_2 molecules near the composite surfaces and may well yield materials for optical sensor devices, for example, optical oxygen-partial-pressure sensors. The detailed results will be described in a separate paper.

Acknowledgments

This work was partially supported by a Grant-in-Aid for Scientific Research from the Ministry of Education, Science, Sports, Culture and Technology, Japan. This work is also partially supported by a Project Research Grant from The Institute of Information Sciences of College of Humanities and Sciences (Nihon University) and by a Cooperative Research Grant from The Institute of Natural Sciences (Nihon University).

References

Bloch R and Möller H 1931 *Z. Phys. Chem.* A **152** 245
Burley G 1963 *Am. Mineral.* **48** 1266
Burley G 1967 *Acta Crystallogr.* **23** 1
Cardona M 1963 *Phys. Rev.* **129** 69
Fujishima A, Rao T N and Tryk D A 2000 *J. Photochem. Photobiol.* C **1** 1
Fujishiro F and Mochizuki S 2003 *ICDS-22: The 22nd Int. Conf. on Defects in Semiconductors;*; *Physica* B submitted
Gupta R K, Agraval R C and Pandey R K 1996 *Solid State Ionics* ed B V R Chowdary *et al* (Singapore: World Scientific) p 499
Hosaka N, Sekiya T and Kurita S 1997 *J. Lumin.* **72–74** 874
Jow T and Wagner J B Jr 1979 *J. Electrochem. Soc.* **126** 1963
Lee J-S, Adams S and Maier J 2000a *Solid State Ion.* **136/137** 1261
Lee J-S, Adams S and Maier J 2000b *J. Phys. Chem. Solids* **61** 1607
Liang C C 1973 *J. Electrochem. Soc.* **120** 1289
Mochizuki S 2001 *Physica* B **308–310** 1042
Mochizuki S and Araki H 2003 *Physica* B submitted
Mochizuki S and Fujishiro F 2002 *Proc 6th Forum on Superionic Conductor Physics* (Kyoto: The Japanese Society of Ion Transport) pp 41–6
Mochizuki S and Fujishiro F 2003 *Phys. Status Solidi* c **0** 763
Mochizuki S, Fujishiro F and Shimizu T 2003 (in preparation)
Mochizuki S, Nakanishi T, Suzuki Y and Ishi K 2001a *Appl. Phys. Lett.* **79** 3785
Mochizuki S and Ohta Y 2000 *J. Lumin.* **87–89** 299
Mochizuki S, Suzuki Y, Nakanishi T and Ishi K 2001b *Physica* B **308–310** 1046
Mochizuki S and Umezawa K 1997 *Phys. Lett.* A **228** 111
Shahi K and Wagner J B Jr 1981 *Solid State Ion.* **3/4** 295
Shastry M C R and Rao K J 1992 *Solid State Ion.* **51** 311
Suisalu A, Aarik J, Mandar H and Sildos I 1998 *Thin Solid Films* **336** 295
Tang H, Berger H, Schmid P E and Levy F 1994 *Solid State Commun.* **92** 267
Uvarov N F, Vanek P, Savinov M, Zelezny V, Studnicka V and Petzelt J 2000 *Solid State Ion.* **127** 253
Watanabe M, Sasaki S and Hayashi T 2000 *J. Lumin.* **87–89** 1234
West A R 1984 *Solid State Chemistry and Its Applications* (New York: Wiley)
Zhao Z-Y, Wang C-Y, Dai S-Y and Chen L-Q 1983 *Solid State Ion.* **9/10** 1175